LBL-34175
UC-413
Preprint

Lawrence Berkeley Laboratory
UNIVERSITY OF CALIFORNIA

Submitted to Physical Review C

Electromagnetic Dissociation of ^{238}U at 120 MeV/Nucleon

M.L. Justice, Y. Blumenfeld, N. Colonna, D.N. Delis,
G. Guarino, K. Hanold, J.C. Meng, G.F. Peaslee,
G.J. Wozniak, and L.G. Moretto

May 1993

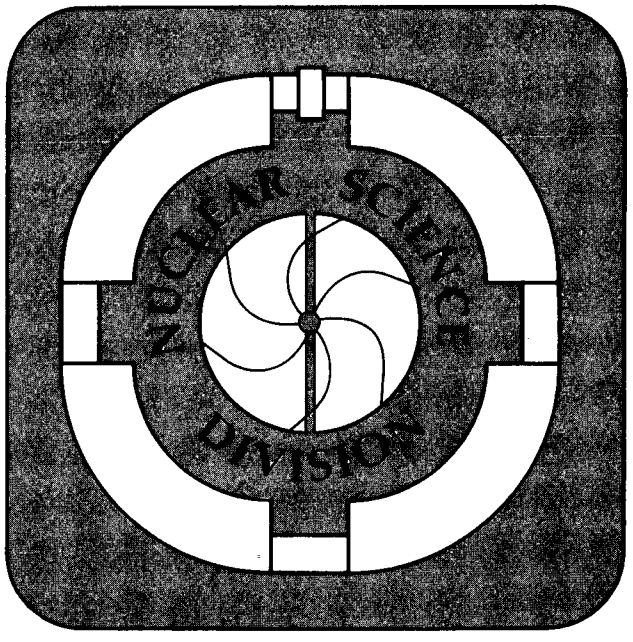

Prepared for the U.S. Department of Energy under Contract Number DE-AC03-

DISCLAIMER

LBL - 34175
UC-413

Electromagnetic Dissociation of ^{238}U at 120 MeV/Nucleon

M.L. Justice, Y. Blumenfeld, N. Colonna, D.N. Delis, G. Guarino, K. Hanold, J.C. Meng, G.F. Peaslee, G.J. Wozniak, and L.G. Moretto

Nuclear Science Division, Lawrence Berkeley Laboratory
University of California, Berkeley, California 94720, USA

May 1993

This work was supported by the Director, Office of Energy Research, Division of Nuclear Physics of the Office of High Energy and Nuclear Physics of the U.S. Department of Energy under Contract DE-AC03-76SF00098

Electromagnetic Dissociation of ^{238}U at 120 MeV/nucleon

M.L. Justice, Y. Blumenfeld*, N. Colonna†, D.N. Delis,
G. Guarino, K. Hanold, J.C. Meng**, G.F. Peaslee††,
G.J. Wozniak, and L.G. Moretto

Lawrence Berkeley Laboratory, Berkeley, California 94720

Electromagnetic fission cross sections of a 120 MeV/nucleon ^{238}U beam incident on five targets: ^{9}Be, ^{27}Al, ^{nat}Cu, ^{nat}Ag, and ^{nat}U; have been extracted from measurements of projectile fission cross sections. The nuclear interaction contributions to the experimentally observed cross sections were determined by extrapolation from the Be target data using a geometrical scaling model. The results are compared to model calculations in which electric quadrupole excitations have been included.

Electromagnetic dissociation (EMD) is a process that occurs when a nucleus is excited above its particle emission threshold by the electromagnetic field of another nucleus as it passes by outside the range of the strong nuclear force. Experimentally, electromagnetic dissociation has been observed with relativistic heavy ions [1-16]. Aside from the emulsion work of Ref. 6 however, these experiments have been restricted to either few nucleon removal from heavy nuclei or several nucleon removal from light nuclei. Here we present the results of the first electronic counter experiment designed to measure electromagnetic fission cross sections of a heavy nucleus. In addition, this was the first measurement of EMD cross sections at a beam energy where

there is predicted to be significant contributions from electric quadrupole excitations.

Fission cross sections of a 120 MeV/nucleon ^{238}U beam incident on five targets (^{9}Be, ^{27}Al, ^{nat}Cu, ^{nat}Ag, and ^{nat}U) were measured at the Lawrence Berkeley Laboratory's BEVALAC. The projectile fission fragments were detected in coincidence by 16 position sensitive ΔE-E telescopes [17]. Each telescope was composed of a 300 μm diffused junction Si ΔE detector followed by a 5 mm Si(Li) E detector. The telescopes were placed concentrically about the beam in two rings of eight telescopes each. The upstream ring intersected the beam axis 37.0 cm downstream of the target and covered the angular region $4.5° \lesssim \theta \lesssim 13.5°$, while the downstream ring intersected the beam axis 103.2 cm downstream of the target and covered $1.5° \lesssim \theta \lesssim 4.5°$. One surface of each silicon detector was divided into fifteen 2.42 mm wide, high conductivity strips separated by .607 mm wide, high resistivity gaps to give position information through the technique of resistive charge division. The strips of the E detectors were rotated 90° with respect to the ΔE strips to give full two dimensional position information with an overall resolution of $\sim$1.5 mm in the x and y directions. The absolute beam flux was measured with a 1/4″ thick plastic scintillator paddle located approximately 150 cm downstream of the target. A complete description of the experimental setup along with the details of the procedure used to calibrate the silicon detectors can be found in Ref. 18.

Pulse height information from the E and ΔE detectors was combined, using a range algorithm [19], to determine the charges of the fragments. The charge resolution obtained varied from approximately $\pm.25$ Z units for the lightest fission fragments to approximately $\pm.5$ Z units for the heaviest fragments. The position information from the Si detectors was used, along with the total energy deposited, to determine the velocity vectors of the fragments.

Raw $Z_1 + Z_2$ distributions for the five targets are shown in Fig. 1. The range

of excitation energies associated with virtual photon absorption is modest (< 20 MeV) at the beam energy of this experiment. Therefore, electromagnetic fission practically always leads to a true charge sum of 92. Of course, the data contain a large background from nuclear interaction processes as well, but the ratio of electromagnetic to nuclear fragmentation increases with the charge of the target nucleus. This can be seen in the increasing sharpness of the peak at $Z_1 + Z_2 = 92$ as Z_{targ} increases in Fig. 1.

Raw Z distributions for $Z_1 + Z_2 = 92$ events are shown in Fig. 2. A smooth transition from primarily symmetric fission for the Be target data to primarily asymmetric fission for the U target data is seen. As is well known from studies of light-particle induced fission, the magnitude of the asymmetric component in fragment yields is a sensitive function of the amount of excitation energy imparted to the fissioning system [20]. Higher excitation energies lead to increased yields of the symmetric component in ^{238}U fission. The increasing importance of the asymmetric fission component as the target atomic number increases is a direct illustration of the onset of the low excitation energy electromagnetic dissociation process.

For the most peripheral events ($Z_1 + Z_2 = 91, 92, 93$), a velocity for the fissioning source was calculated assuming two body decay:

$$\vec{\beta}_s = \frac{\vec{P}_s}{[P_s^2 + M_s^2]^{1/2}} , \tag{1}$$

where $\vec{P}_s \equiv \vec{p_1} + \vec{p_2}$ and $M_s \equiv M_1 + M_2$. Plots of the parallel and transverse components of $\vec{\beta}_s$ for $Z_1 + Z_2 = 92$ events are shown in Fig. 3. Although the $\beta_{||}$ distributions for the five targets look very similar, the $\beta_\perp$ distributions shift to larger values as the target atomic number increases. This behavior can be explained as being due to the increasing Coulomb kick the projectile receives from the target by the Rutherford scattering term in the potential. The arrows in Fig. 3(b) indicate the calculated

transverse velocities at grazing impact parameters, assuming classical Rutherford trajectories.

The geometrical acceptances of the detector system for coincidence events leading to charge sums of 91, 92, and 93 were calculated with a Monte Carlo program. The fragments were assumed to be emitted isotropically in the projectile rest frame with kinetic energies taken from measurements on proton-induced ^{238}U fission [21]. A grid of 20 × 20 points covering the measured range of $\beta_\perp$ vs. $\beta_\parallel$ was set up and 100,000 events for each $Z_1 - Z_2$ split were generated at each point. Coincidence efficiencies at other values of $\vec{\beta}_s$ were determined by interpolation. Total fission cross sections for $Z_1 + Z_2 = 92$ events in mb were then calculated from the relation:

$$\sigma^f_{92} = \sum_{i,j=92-i} \frac{n_{ij} \cdot A}{\epsilon_{ij} \cdot F \cdot \Delta x \cdot N_A} \cdot 10^{30} \,, \tag{2}$$

where n_{ij} and ϵ_{ij} are the number of detected events and coincidence efficiency for $Z_1 = i$, $Z_2 = j$ as a function of $\vec{\beta}_s$, A is the atomic weight of the target, F is the integrated beam flux, Δx is the thickness of the target in mg/cm^2, and N_A is Avogadro's number. Total fission cross sections for $Z_1 + Z_2 = 91$ and $Z_1 + Z_2 = 93$ events were calculated from similar expressions.

Due to the imperfect charge resolution of our detectors, we cannot give reliable values for the cross sections into individual fragmentation channels. Detailed Monte Carlo studies of the effects of charge misidentification were made, however, and it was found that the sum cross sections:

$$\sigma^f_\Sigma = \sigma^f_{91} + \sigma^f_{92} + \sigma^f_{93} \,, \tag{3}$$

were relatively insensitive (< 6%) to fragment Z misidentification [18]. Moreover, it was determined that < 5% of the true $Z_1 + Z_2 = 92$ events were misidentified by more than one charge sum unit, indicating that nearly all of the electromagnetic fission events are included in σ^f_Σ.

The sum cross sections include a nuclear interaction component as well as the EMD component:

$$\sigma_{\Sigma}^{f} = \sigma_{\mathrm{EMD}}^{f} + \sigma_{\mathrm{NUC}}^{f} \,. \tag{4}$$

Under the conditions of this experiment, the cross section for the Be target data is expected to be almost entirely due to nuclear interaction. The nuclear cross sections for the other four targets were determined from the Be data using a geometrical scaling model:

$$\sigma_{\mathrm{NUC}}^{geom} = 2\pi \left(b_{min} - a - \frac{\Delta b}{2} \right) \Delta b \,, \tag{5}$$

where

$$a = \frac{Z_p Z_t e^2}{\mu \beta^2 \gamma} \,, \tag{6}$$

corrects for the Rutherford bending of the trajectory [18]. Using the parameterization [22]:

$$b_{min} = 1.34 \left[A_p^{1/3} + A_t^{1/3} - .75 \left(A_p^{-1/3} + A_t^{-1/3} \right) \right] \,, \tag{7}$$

and the measured cross section of 494 ± 11 mb for the Be data, Δb was determined to be: $\Delta b = .80 \pm .04$ fm.

The EMD fission cross sections obtained by subtracting off the extrapolated nuclear cross sections are listed in Table I and plotted in Fig. 4. The error bars for the Al, Cu, and Ag target cross sections were calculated from the statistical uncertainties plus the best estimate of the uncertainties introduced by fragment charge misidentification. The large error on the U target point includes an additional uncertainty introduced by problems with the beam flux counter during this run. All errors are 1σ. The overall normalization uncertainty of Fig. 4 is estimated to be $\pm 20\%$.

A framework for calculating EMD cross sections is given by the equivalent photon approximation [23] :

$$\sigma_{\rm EMD} = \int d\omega \sigma_\gamma(\omega)\, N(\omega)\ , \tag{8}$$

where $\sigma_\gamma(\omega)$ is the appropriate photodissociation cross section for the fragmenting nucleus and $N(\omega)$ is the virtual photon spectrum generated by the other nucleus.

The simplest form of the virtual photon spectrum is given by the Weizsäcker-Williams (WW) approximation [24]. In the WW approach the classical electromagnetic fields are approximated as two pulses of plane waves. The resulting number spectrum of virtual photons per unit photon energy interval, integrated over impact parameters, is given by:

$$N^{WW}(\omega) = \frac{2Z^2\alpha}{\pi\omega\beta^2}\left[\xi K_0(\xi) K_1(\xi) - \frac{\beta^2\xi^2}{2}\left(K_1^2(\xi) - K_0^2(\xi)\right)\right]\ , \tag{9}$$

where ω is the virtual photon energy, Z is the charge of the nucleus emitting the virtual photon, β is the relative velocity of the two nuclei, $K_0(K_1)$ is the modified Bessel function of order zero(one), $\xi = \omega b_{min}/\beta\gamma$, and b_{min} is the cutoff impact parameter, below which nuclear fragmentation processes take over and electromagnetic dissociation ceases to be important.

An approach that goes beyond the WW approximation has been given by Alder and Winther [25], and later put into the context of the virtual photon language by Bertulani and Baur [26]. In this approach, a proper multipole expansion of the electromagnetic field is made and an analytical expression for the equivalent photon numbers of all multipolarities is obtained. Eq. (8) is then modified to read:

$$\sigma_{\rm EMD} = \sum_{\pi l} \int d\omega \sigma_\gamma^{\pi l}(\omega)\, N^{\pi l}(\omega)\ , \tag{10}$$

where $\sigma_\gamma^{\pi l}(\omega)$ is the photodissociation cross section for real photons of multipolarity πl. The expression for $N^{E1}(\omega)$ in this multipole expansion method is identical to $N^{WW}(\omega)$, while the E2 spectrum is given by [26] :

$$N^{E2}(\omega) = \frac{2Z^2\alpha}{\pi\omega\beta^4}\left[2\left(1-\beta^2\right)K_1^2 + \left(2-\beta^2\right)^2 \xi K_0 K_1 - \frac{\xi^2\beta^4}{2}\left(K_1^2 - K_0^2\right)\right]\ , \tag{11}$$

where all K's are functions of ξ as in Eq. (9). In the high energy limit, as $\beta \rightarrow 1$, Eq. (11) becomes equivalent to Eq. (9). In fact, this is true in general; as the velocity of the projectile approaches the speed of light, the virtual photon spectra for all multipolarities become equivalent to the E1 spectrum. At lower relative velocities, however, $N^{E2}(\omega)$ can be significantly enhanced in comparison to $N^{WW}(\omega)$.

The curves in Fig. 4 are the results of two model calculations. The lower, dashed curve is the prediction of the WW approximation with the parameterization of Eq. (7) for b_{min}. The total photofission cross section was taken from Ref. 27. The upper, solid curve was calculated by summing over E1 and E2 multipoles using Eq. (10). The E2 photoabsorption cross section was assumed to be of the form [28] :

$$\sigma_{\gamma}^{E2}(\omega) = \frac{8\pi^3\alpha}{150\,(\hbar c)^2}\,\omega^3\,\frac{dB^{E2}}{d\omega}\,, \tag{12}$$

with the following form for the strength function, $dB^{E2}/d\omega$,

$$\frac{dB^{E2}}{d\omega} = \frac{K}{\omega}\frac{\Gamma^2}{\left(\omega^2-\omega_0^2\right)^2+\omega^2\Gamma^2}\,. \tag{13}$$

The value of K was determined by assuming that the E2 cross section exhausts 100% of the energy-weighted sum rule [28] :

$$\int d\omega\omega\frac{dB^{E2}}{d\omega} = \frac{25\hbar^2Z^2}{4\pi AM}\left\langle R^2\right\rangle\,, \tag{14}$$

where M is the nucleon mass, Z and A are the charge and mass number of ^{238}U, and $\langle R^2\rangle$ is its mean square charge radius. The numerical value of the right hand side of this equation was taken to be 1.00×10^5 MeV fm^4 [29]; ω_0 and Γ were taken to be 10 MeV and 3.5 MeV, respectively [30].

The E2 photofission cross section is related to the total E2 photoabsorption cross section by:

$$\sigma_{\gamma,f}^{E2}(\omega) = P_f^{E2}(\omega)\sigma_{\gamma}^{E2}(\omega)\,, \tag{15}$$

where $P_f^{E2}(\omega)$ is the E2 fission probability as a function of photon energy. The parameterization:

$$P_f^{E2}(\omega) = a - \frac{b}{1 + e^{(\omega - c)/d}} , \tag{16}$$

with $a = 0.4$, $b = 0.18$, $c = 13.4$ MeV, and $d = 0.59$ MeV was used for $P_f^{E2}(\omega)$. This parameterization reproduces the total fission probability as measured in photonuclear experiments [31]. The recoil correction to the equivalent photon numbers [25]:

$$b_{min} \longrightarrow b_{min} + \frac{\pi}{2} a , \tag{17}$$

where a is given by Eq. (6), was included in both of the calculations of Fig. 4.

While the measured cross sections are seen to increase with Z_{targ} in Fig. 4, the quantitative agreement with the model calculations is not good. The Al, Cu, and Ag data points have approximately the correct Z_{targ} dependence but lie well above the theoretical predictions, while the U point is clearly too low in relation to the other points. A 2σ shift upward of the U point gives the data approximately the same shape as the solid curve, only too high by $\sim 50\%$ — well above the estimated normalization uncertainty. The theoretical calculations are quite sensitive to the cutoff impact parameters, however, so some of the discrepancy could be eliminated by simply adjusting the b_{min} values downward. For example, changing the number outside of the brackets in Eq. (7) from 1.34 to 1.10 shifts the solid curve of Fig. 4 up into good agreement with the Al, Cu, and Ag points. The $\sigma_{\rm NUC}$ values calculated from the geometrical model would also be affected by such a change in the b_{min} values, but this effect could be offset by adjusting Δb in the opposite direction.

A potentially important deficiency of the models is their neglect of nuclear deformation effects. For a ^{238}U projectile incident on a spherical target, the effect would enter through a dependence of b_{min} on the particular orientation of the projectile. In the case where the target is also deformed there could be an additional effect on

the multipole structure of the fields generated by the target. A proper treatment of these two effects would involve a complicated averaging over the various possible orientations of the projectile and target and has not been attempted. Qualitatively, however, it is clear that the first effect would serve to increase the theoretical predictions, since allowing b_{min} to depend on orientation increases the number of events at smaller impact parameters. As for the second effect, it is not obvious in which direction or by how much the various equivalent photon numbers would be shifted but if, for example, $N^{E1}(\omega)$ is decreased at the expense of higher multipoles then the cross section for a deformed target would go down.

In summary, we have demonstrated a new technique for studying the electromagnetic dissociation process. The trend in fragment mass asymmetries of Fig. 2 provides conclusive evidence of an electromagnetic component to the total fission cross sections of ^{238}U at 120 MeV/nucleon. While the extracted electromagnetic fission cross sections seem to favor calculations which include electric quadrupole excitations, more work in both experiment and theory is needed in order to understand the shape of the dependence of $\sigma_{\rm EMD}$ on target atomic number.

This work was supported by the Director, Office of Energy Research, Division of Nuclear Physics of the the Office of High Energy and Nuclear Physics of the U.S. Department of Energy under Contract DE-AC03-76SF00098.

TABLES

TABLE I. Experimental and calculated EMD fission cross sections (mb).

target	σ_{exp}	σ_{WW}	σ_{E1+E2}
Al	78 ± 30	27	33
Cu	246 ± 37	99	120
Ag	393 ± 42	204	248
U	568 ± 127	504	613

REFERENCES

* Present address: Institute de Physique Nucleaire, Orsay, France

† Present address: INFN, Bari, Italy

** On leave from the Institute of Atomic Energy, Beijing, China

†† Present address: NSCL, MSU, East Lansing, MI 48844

[1] H.H. Heckman and P.J. Lindstrom, Phys. Rev. Lett. **37**, 56 (1976).

[2] G.D. Westfall *et al.*, Phys. Rev. C **19**, 1309 (1979).

[3] D.L. Olson *et al.*, Phys. Rev. C **24**, 1529 (1981).

[4] M.T. Mercier *et al.*, Phys. Rev. Lett. **52**, 898 (1984).

[5] M.T. Mercier *et al.*, Phys. Rev. C **33**, 1655 (1986).

[6] L.F. Canto *et al.*, Phys. Rev. C **35**, 2175 (1987).

[7] J.C. Hill *et al.*, Phys. Rev. Lett. **60**, 999 (1988).

[8] J.C. Hill *et al.*, Phys. Rev. C **38**, 1722 (1988).

[9] P.B. Price *et al.*, Phys. Rev. Lett. **61**, 2193 (1988).

[10] C. Brechtmann and W. Heinrich, Z. Phys. A **330**, 407 (1988).

[11] C. Brechtmann and W. Heinrich, Z. Phys. A **331**, 463 (1988).

[12] J.C. Hill *et al.*, Phys. Rev. C **39**, 524 (1989).

[13] C. Brechtmann *et al.*, Phys. Rev. C **39**, 2222 (1989).

[14] G. Baroni *et al.*, Nuc. Phys. **A516**, 673 (1990).

[15] D.L. Olson *et al.*, Phys. Rev. C **44**, 1862 (1991).

[16] J.C. Hill *et al.*, Phys. Lett. B **273**, 371(1991).

[17] W.L. Kehoe *et al.*, Nucl. Instr. and Meth. **A311** 258 (1992).

[18] M.L. Justice, Ph.D. thesis, University of California, Berkeley 1991; Lawrence Berkeley Laboratory Report LBL-31704.

[19] F.S. Goulding and B.G. Harvey, Ann. Rev. Nuc. Sci. **25**, 167 (1975).

[20] R. Vandenbosch and J.R. Huizenga, *Nuclear Fission* (Academic Press, New York, 1973).

[21] R.L. Ferguson *et al.*, Phys. Rev. C **7**, 2510 (1973).

[22] C.J. Benesh *et al.*, Phys. Rev. C **40**, 1198 (1989).

[23] C.A. Bertulani and G. Baur, Phys. Rep. **163**, 299 (1988).

[24] C.F. Weizsäcker, Z. Phys. **88**, 612 (1934).
E.J. Williams, Phys. Rev. **45**, 729 (1934).

[25] A. Winther and K. Alder, Nucl. Phys. **A319**, 518 (1977).

[26] C.A. Bertulani and G. Baur, Nucl. Phys. **A442**, 739 (1985).

[27] J.T. Caldwell *et al.*, Phys. Rev. C **21** 1215 (1980).

[28] J.S. O'Connell, Proc. Int. Conf. on Photonuclear Reactions and Applications, ed. B.L. Berman (Lawrence Livermore Laboratory, Livermore, CA, 1973) p. 71.

[29] Th. Weber *et al.*, Phys. Rev. Lett. **59**, 2028 (1987).

[30] J.D.T. Arruda-Neto and B.L. Berman, Physica Scripta **40**, 735 (1989).

[31] A. Veyssière *et al.*, Nucl. Phys. **A199**, 45 (1973).

FIGURES

FIG. 1. Raw $Z_1 + Z_2$ distributions.

FIG. 2. Raw Z distributions for $Z_1 + Z_2 = 92$ events.

FIG. 3. (a)Parallel source velocities for $Z_1 + Z_2 = 92$ events. The arrows mark the beam velocity. (b)Transverse source velocities for $Z_1 + Z_2 = 92$ events. The arrows mark the calculated transverse velocities assuming classical Rutherford trajectories at $b = b_{min}$.

FIG. 4. Experimental EMD cross sections (symbols). The dashed curve is the WW prediction. The solid curve was obtained by summing over E1 and E2 multipoles. The log-log plot emphasizes the approximate Z_{targ} dependence contained in Eq.s (9) and (11).

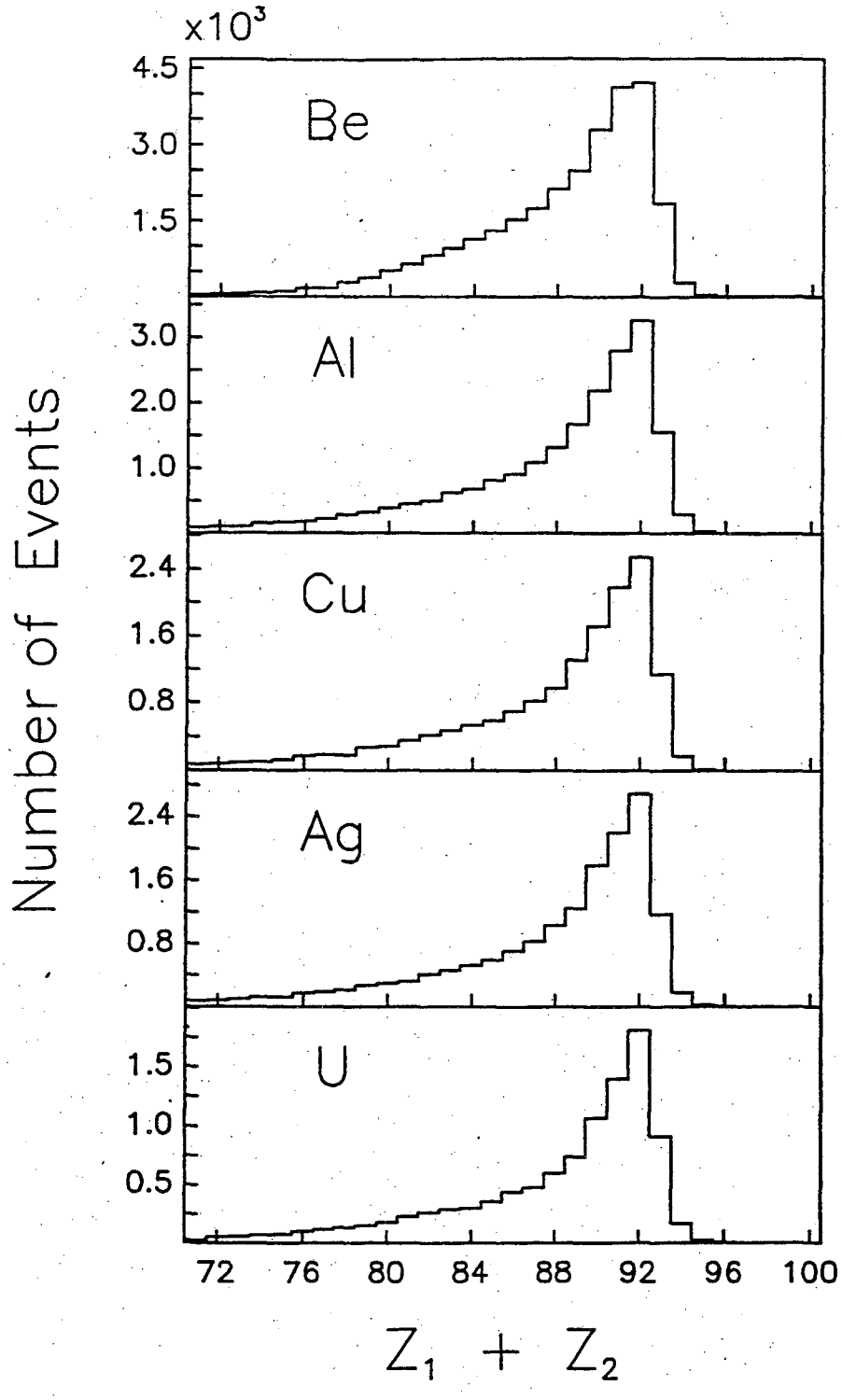
x10³
4.5
3.0
1.5
Be
3.0
2.0
1.0
Al
2.4
1.6
0.8
Cu
2.4
1.6
0.8
Ag
1.5
1.0
0.5
U
Number of Events
72
76
80
84
88
92
96
100
Z1 + Z2
XBL 934-569

fig. 1

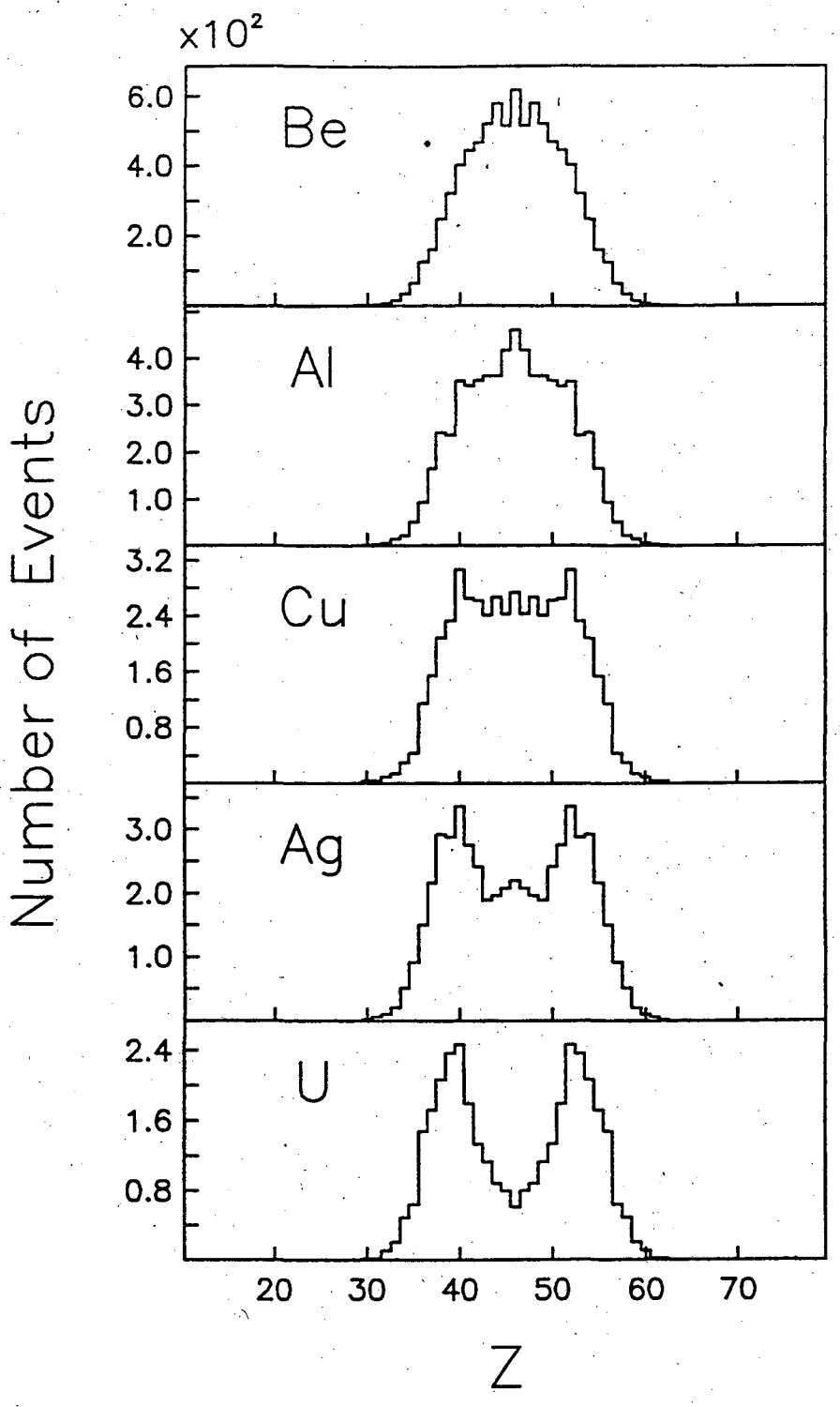

fig. 2

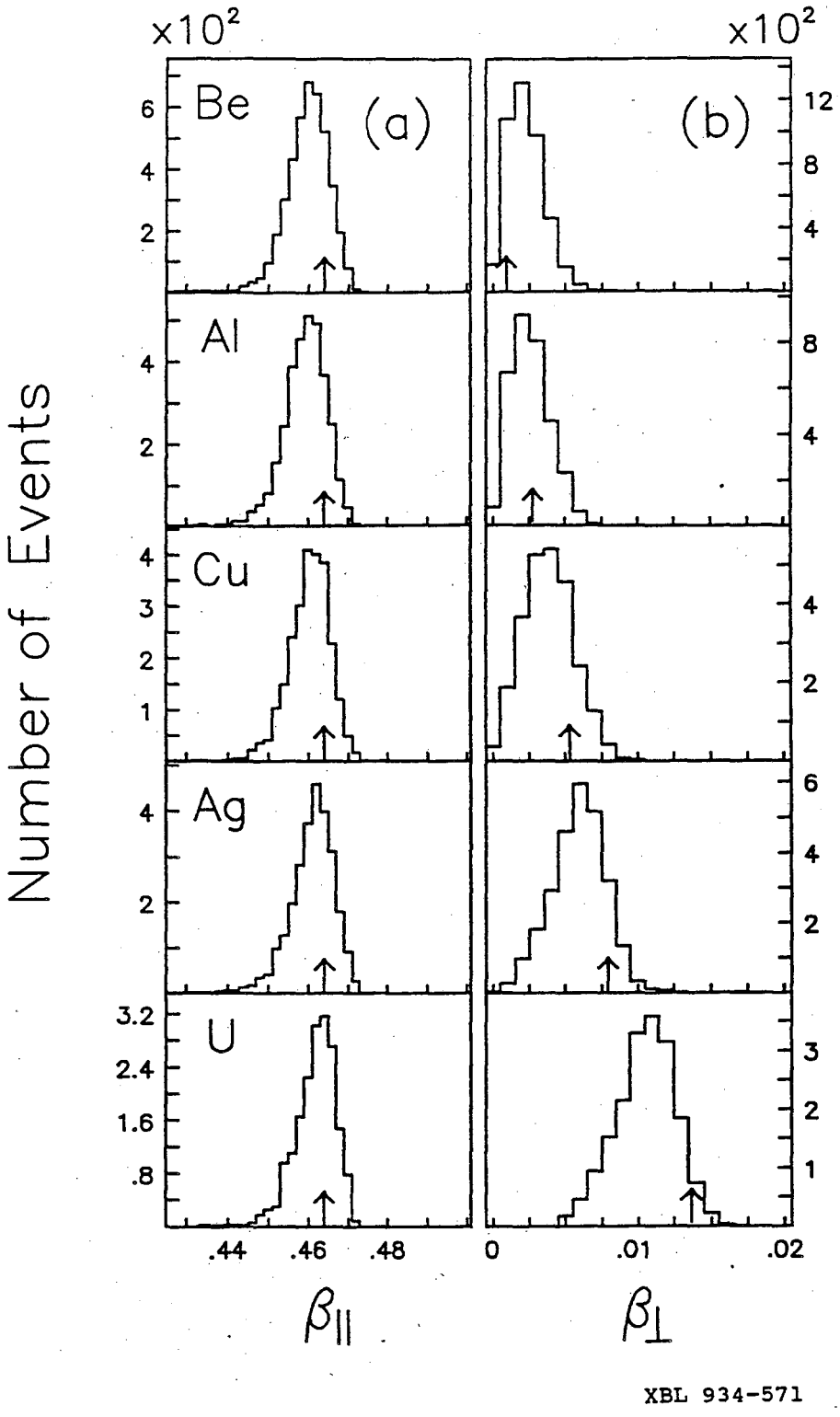
x10²
x10²
Be
(a)
(b)
Al
Cu
Ag
U
Number of Events
.44
.46
.48
0
.01
.02
β||
β⊥
XBL 934-571

fig. 3

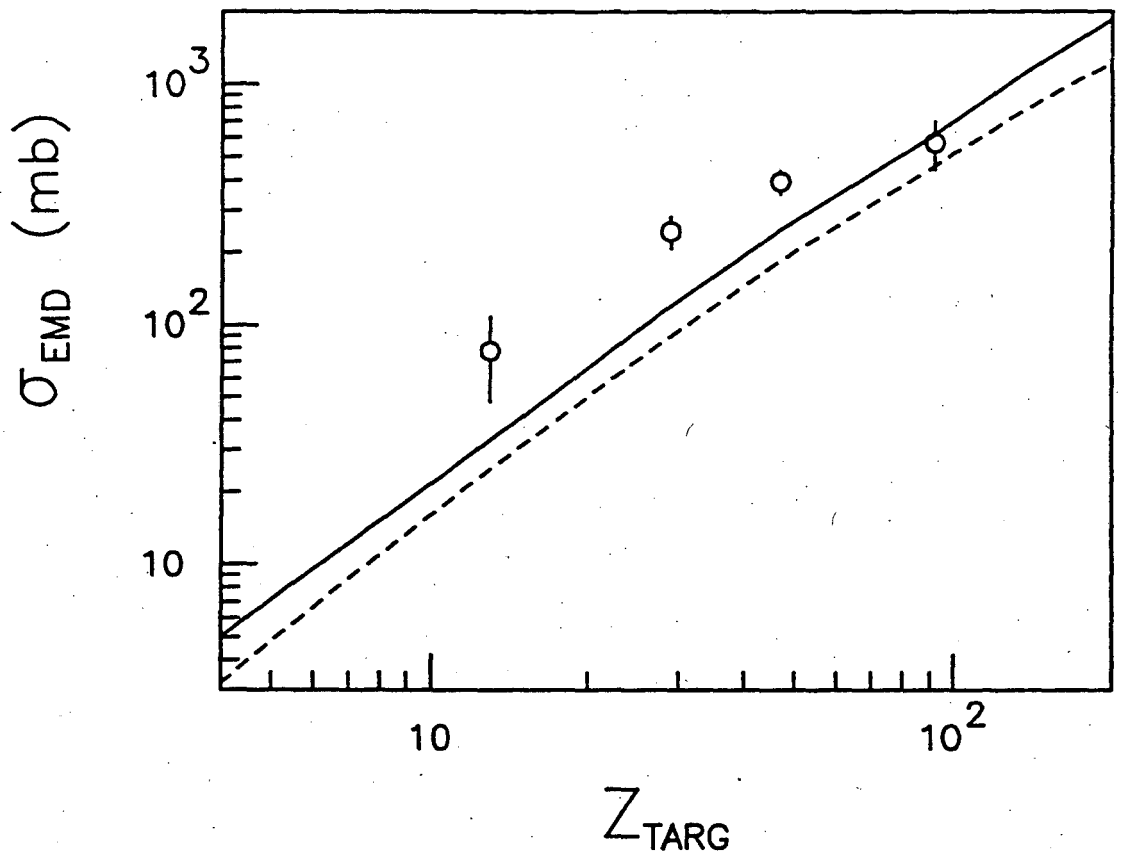

XBL 934-572

fig. 4

LAWRENCE BERKELEY LABORATORY
UNIVERSITY OF CALIFORNIA
TECHNICAL INFORMATION DEPARTMENT
BERKELEY, CALIFORNIA 94720